X-ray Beamlines at Superconducting Wavelength Shifter

NSRRC has installed a specially designed Superconducting Wavelength Shifter (SWLS) insertion device in the storage ring to extend the synchrotron radiation spectrum to the hard X-ray region. This SWLS, composing of three magnet poles with a maximum magnetic field strength of 6 Tesla, shifts the photon critical energy of the synchrotron radiation from 2 to 9 keV. And hence it provides a photon flux 7×10^{11} photons s^{-1} $mrad^{-1}$ $0.1\%BW^{-1}$ $200mA^{-1}$, which is 70 times as large as that of the currently operated 1.8 Tesla wiggler source at 30 keV (see the respective figure in the article by C. S. Hwang, Facility Highlights). To fully utilize the total available horizontal radiation fan of 20 mrad from the SWLS source, we have constructed three hard X-ray beamlines, BL01A, BL01B, and BL01C, as shown in Fig.1. BL01A is a white light beamline for X-ray image applications. BL01B, covering energies from 5 to 20 keV, is for scattering experiments, whereas BL01C, covering photon energies from 6 to 33 keV, is ideal for EXAFS and X-ray diffraction (XRD) experiments.

BL01A collects 1 mrad from the right wing-tip of the horizontal radiation fan. The beam, gated by a water-cooled aperture, passes two 250 μm Be-windows located at 11.9 m and hutch entrance of the end-station, respectively. Currently, this beamline serves for the development of medium-resolution phase-contrast X-ray imaging experiments. The spatial resolution of a phase-contrast X-ray imaging system is 1 m. And within 10 ms, the BL01A's photon flux can saturate a camera of 700-microns field-of-view. The X-ray image of an electron gun of the Cathode Radiation Tube (CRT) monitor was measured for testing the performance of this system. Even being packed, the tungsten filament and the protecting oxide layer can still be distinguished clearly. Furthermore, the detailed internal structure of the head of a fruit fly was observed, demonstrating vividly that the phase-contrast X-ray imaging technique can be used in revealing the internal structures of materials of low atomic numbers or biomaterials, that is strongly needed in live science and medical studies.

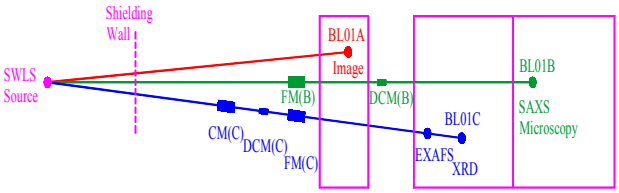

Fig. 1: Top view of the optical layout of Supper-conducting Wavelength Shifter (SWLS) beamlines BL01A, BL01B and BL01C. CM: Collimating Mirror. DCM: Double Crystal Monochromator. FM: Focusing Mirror. EXAFS: Extended X-ray Absorption Fine Structure. XRD: X-ray Diffraction. SAXS: Small Angle X-ray Scattering.

BL01B takes the central 3 mrad of the horizontal radiation fan. The beam is focused by a water-cooled toroidal focusing mirror FM(B), located at 15.5 m, with a nearly 1:1 condition onto the sample position at 30.2 m. The glancing incident angle of the beam on FM(B), coated with Rh, is chosen as 3.2 mrad to provide an optimized reflectivity of 90% and a cutoff energy at 21 keV. For a monochrome beam, A Ge (111) double crystal monochromator DCM(B) located at 20.8 m is used to select photon energy of the beam. In the very near future, an advanced X-ray nano-microscope will be installed in the BL01B end-station. Currently, a Small Angle X-ray Scattering (SAXS) instrument end-station is setup for several applications, including polymer systems, bio-molecules in solution, and the structural evolution of alloys at high temperature.

The energy-resolution of BL01B is mainly dominated by source vertical divergence, because there is no collimating mirror adopted in this beamline. Therefore, the energy-resolution $\Delta E/E$ is as large as 1×10^{-3}. However, the photon flux of this beamline is optimized. The photon flux measured with an ion chamber filled with 1 atm nitrogen gas is shown in Fig. 2. The average photon flux is

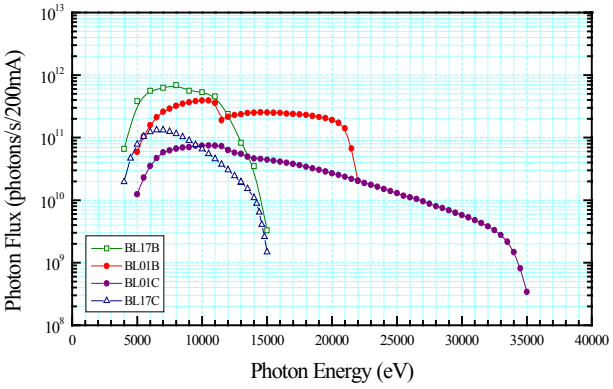

Fig. 2: Measured photon flux at the sample position of super-conducting wavelength shift beamlines BL01B, BL01C and wiggler beamlines BL17B, BL17C.

3×10^{11} photons/s with 200 mA ring current. The flux measured is shy to the calculated value by a factor of 2.5, but outcasts the flux of the wiggler beamline BL17B by 77 times at 15 keV. The measured focused beam dimensions are 1.5 mm× 0.5 mm, with divergent angles 1.5 and 0.3 mrad in the horizontal and vertical directions, respectively.

Further, we have measured the best Q-resolution of BL01B for granting to the small angle X-ray scattering (SAXS) setup. Using an Ag-behenate sample, the SAXS profiles extracted from the IP images with photon energies 10.35 keV and 22.11 keV, respectively, are shown in Fig. 3. The line at Q = 0.75 Å^{-1} ($Q = 4\pi \sin\theta_B/\lambda$, where θ_B is Bragg angle and λ is wavelength of incident beam), fitted with a Gaussian profile, demonstrates a good $\Delta Q/Q$ resolution of 0.46% can be achieved.

The unprecedented energy spectrum of the SWLS source grants the opportunity for resolving multi-phase structures with anomalous X-ray scattering. In Fig. 4, we show anomalous small angle X-ray scattering (ASAXS) for the Pt/Ru nano-particles embedded in fine carbon grains for fuel-cell applications, performed near 11.5 keV and 22.1 keV for the L and K absorption edges of Pt and Ru. With the Ru resonant energy 22.1 keV, the SAXS profile measured drops, in the lower-Q region (see the arrow), than that measured at others energies, indicating that Ru dominates the shell structure of the Pt-Ru nanoparticles. On the other hand, with photon energy near the L_3 edge of Pt, the SAXS profile (see the inset) drops, in the higher-Q region, from that measured at other energies, demonstrating clearly that Pt dominates the core structure of the Pt-Ru nanoparticles.

BL01C takes 2 mrad from the left wingtip of the horizontal radiation fan. The beam is collimated by a cylindrical mirror CM(C) located at 11 m, monochormated by a Si(111) double crystal monochromator DCM(C) located at 13.3 m, and subsequently focused by a toroidal mirror FM(C) located at 15.5 m, before focusing at the XRD end station. Both CM(C) and FM(C) are coated with Pt and their glancing incident angles are both chosen as 2.5 mrad to provide a cutoff energy 33 keV. Two spectrometers for EXAFS (BL01C1) and XRD (BL01C2), are installed inside the experimental hutch, which take turns for being fed with photons.

The photon flux of BL01C measured with an ion chamber filled with 1 atm nitrogen gas is shown in Fig. 2. The average photon flux is 2×10^{10} photons/s at 200 mA ring current, which is smaller than the calculated values by a factor of 3.5. The focused beam size measured at the XRD end station is 1.2 mm×0.6 mm.

The energy-resolution of BL01C was extracted from the rocking curves of the second crystal of the DCM. It can be deduced from $\Delta E/E = \cot\theta_B \Delta\theta$, where the angle divergence $\Delta\theta$ is the full width at half maximum of the measured rocking curves. The angle divergence is contributed from the convolution term of Darwin width of two crystals, beam divergence, and acceptant-angle of the detector. In practice, the experimental energy-resolution at the normal operation mode, $(\Delta E/E)_{exp}$, i.e. measured at sample position by scanning both crystals accordingly, is determined by $\cot\theta_B \Delta\theta_{exp}$, with $\Delta\theta_{exp}$ obtained by removing the convolution term of Darwin width of two crystals from $\Delta\theta$.The result appears in Fig. 5, energy-resolution $(\Delta E/E)_{exp}$ is

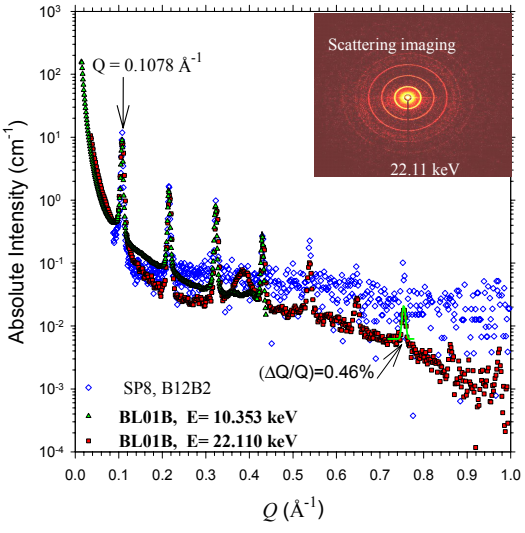

Fig. 3: Small angle X-ray scattering of an Ag-behenate sample.

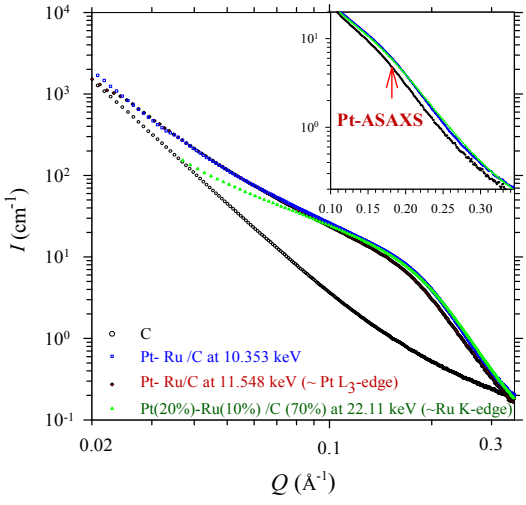

Fig. 4: Anomalous small angle X-ray scattering of the Pt/Ru nano-particles embedded in fine carbon grains for fuel cell applications.

between 1.7×10^{-4} and 3.0×10^{-4} when all the vertical slits are full open. A collimating mirror in a DCM beamline is intentionally used to eliminate the source vertical divergence term. However, a long tangential cylindrical mirror causes an imperfect collimating condition due to the mirror shape and length. Furthermore, any figure error or misalignment of the mirror increases the beam divergence. We use the Shadow ray-tracing program to estimate the total beam divergence including the source size effect. It turns out that the beam divergence contributes significantly to the energy resolution, as can be perceived by the observations with the vertical slit, located right after the DCM, opened symmetrically for 100%, 80% and 50% of total flux (as shown in different color dots). We use the smaller slit opening to cut down the effective mirror length, thus, lower down the beam divergence for a better energy resolution. Small slit opening improves resolution effectively in high energies but makes no improvement at energies near 5 keV. After removing the convolution term of Darwin width of the second crystal, the measured energy-resolution matches well with the estimated values shown by the solid curves in Fig. 5.

The performance of BL01C was further tested with in-situ EXAFS and XRD measurements. The in-situ EXAFS was employed to investigate the genesis of Pd clusters in micro-emulsion system from K_2PdCl_6 precursor for the cluster formation mechanism. We measured EXAFS at Pd K-edge with different amount of the reducing agent (N_2H_5OH), analyzed the k^2-weighted EXAFS data, and then obtained the radius distribution function (RDF) from the Fourier transformation. The result indicates that only Pd-Cl bonds can be observed at the very beginning. Addition of reducing agent leads to progressive reduction of Pd species to metallic state. The increasing of Pd-Pd coordination contribution while decreasing of the Pd-Cl bond contribution, with increasing dosage of reducing agent, implies the formation of Pd clusters. The excellent signal-to-noise ratio conveys to the clear EXAFS oscillations that are discernible up to 14 $Å^{-1}$.

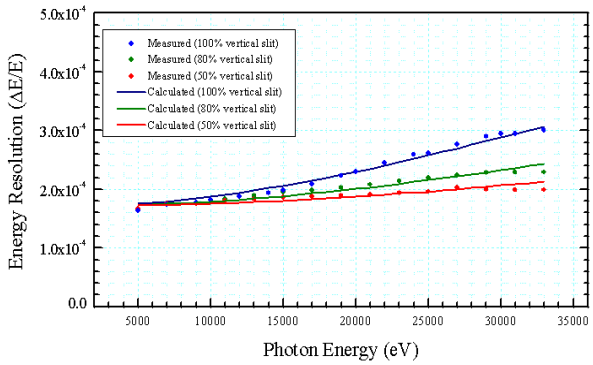

Fig. 5: *Energy resolution (△E/E) of beamline BL01C.*

The high energy XRD of $KNiF_3$ powder sealed in a 0.3 mm capillary was measured at 28 keV. The result shows a very low background XRD pattern recorded by a curved imaging plate with curvature 280 mm for a typical 10 min exposure time. A high-resolution powder diffraction pattern of a quartz sample was also collected at 12 keV with the same setup; the finger print pattern of the spectrum was well resolved. These results demonstrate that this end station is good for high energy and high-resolution XRD experiments, and it is currently set up for studies in several systems including diluted samples.

In summary, optimizing the use of new SWLS source, we have delivered three hard X-ray beamlines for the end-stations designed for X-ray imaging, X-ray scattering, X-ray microscopy, X-ray absorption, and XRD studies. The performances of these beamlines are as good as their designed values and they are now released for beamline applications. These beamlines with unprecedented energy spectrum in National Synchrotron Radiation Research Center certainly opens up more and new opportunities in spectrometers and research fields.

We thank all NSRRC staffs, especially those members of Beamline Group and X-ray Group, and also Dr. C. C. Kuo and Dr. C. H. Lee for their kind assistance. Special thank is given to Dr. C. S. Hwang for providing the data and figures of the SWLS device. We would like to express our gratitude to Dr. Y. Hwu and Mr. W. L. Tsai for providing the figures of X-ray image measured at BL01A.

AUTHORS

Y. F. Song, C. H. Chang, C. Y. Liu, S. H. Chang, U.-S. Jeng, Y. H. Lai, D. G. Liu, J. F. Lee, H. S. Sheu, M. T. Tang, K. L. Tsang, and K. S. Liang
National Synchrotron Radiation Research Center, Hsinchu, Taiwan

PUBLICATIONS

· Y. F. Song, C. H. Chang, C. Y. Liu, L. J. Huang, S. H. Chang, J. M. Chung, S. C. Chung, P. C. Tseng, J. F. Lee, K. L . Tsang, and K. S. Liang, Synchrotron Radiation Instrumentation: 8th International Conference, American Institute of Physics, **412** (2004).

· C. I. Ma, C. H. Chang, L. J. Huang, C. C. Chen, P. C. Tseng, H. S. Fung, S. C. Chung, S. Y. Perng, D. J. Wang, Y. C. Jean, K. L. Tsang, and C. T. Chen, Eighth International Conference on Synchrotron Radiation Instrumentation 2003 (SRI 2003).

CONTACT E-MAIL

song@nsrrc.org.tw